

Sensitivity of pair statistics on pair potentials in many-body systems

Cite as: J. Chem. Phys. 153, 124106 (2020); <https://doi.org/10.1063/5.0021475>

Submitted: 10 July 2020 . Accepted: 04 September 2020 . Published Online: 23 September 2020

Haina Wang , Frank H. Stillinger , and Salvatore Torquato 



View Online



Export Citation



CrossMark



Your Qubits. Measured.

Meet the next generation of quantum analyzers

- Readout for up to 64 qubits
- Operation at up to 8.5 GHz, mixer-calibration-free
- Signal optimization with minimal latency

[Find out more](#)

 Zurich
Instruments

Sensitivity of pair statistics on pair potentials in many-body systems

Cite as: J. Chem. Phys. 153, 124106 (2020); doi: 10.1063/5.0021475

Submitted: 10 July 2020 • Accepted: 4 September 2020 •

Published Online: 23 September 2020



View Online



Export Citation



CrossMark

Haina Wang,¹ Frank H. Stillinger,¹ and Salvatore Torquato^{2,a)}

AFFILIATIONS

¹ Department of Chemistry, Princeton University, Princeton, New Jersey 08544, USA

² Department of Chemistry, Department of Physics, Princeton Center for Theoretical Science, Princeton Institute for the Science and Technology of Materials, and Program in Applied and Computational Mathematics, Princeton University, Princeton, New Jersey 08544, USA

^a) Author to whom correspondence should be addressed: torquato@electron.princeton.edu

ABSTRACT

We study the sensitivity and practicality of Henderson's theorem in classical statistical mechanics, which states that the pair potential $v(r)$ that gives rise to a given pair correlation function $g_2(r)$ [or equivalently, the structure factor $S(k)$] in a classical many-body system at number density ρ and temperature T is unique up to an additive constant. While widely invoked in inverse-problem studies, the utility of the theorem has not been quantitatively scrutinized to any large degree. We show that Henderson's theorem has practical shortcomings for disordered and ordered phases for certain densities and temperatures. Using proposed sensitivity metrics, we identify illustrative cases in which distinctly different potential functions give very similar pair correlation functions and/or structure factors up to their corresponding correlation lengths. Our results reveal that due to a limited range and precision of pair information in either direct or reciprocal space, there is effective ambiguity of solutions to inverse problems that utilize pair information only, and more caution must be exercised when one claims the uniqueness of any resulting effective pair potential found in practice. We have also identified systems that possess virtually identical pair statistics but have distinctly different higher-order correlations. Such differences should be reflected in their individually distinct dynamics (e.g., glassy behaviors). Finally, we prove a more general version of Henderson's theorem that extends the uniqueness statement to include potentials that involve two- and higher-body interactions.

Published under license by AIP Publishing. <https://doi.org/10.1063/5.0021475>

I. INTRODUCTION

The relationship between microscopic forces and the structure of matter is of fundamental interest in classical statistical mechanics and underlies the study of bottom-up material design,^{1–3} fluid and solvation models,^{4,5} and biological molecules.^{6–8} An important theorem due to Henderson states that in a classical many-body system, the pair potential $v(r)$ that gives rise to a given equilibrium pair correlation function $g_2(r)$ at fixed number density ρ and temperature $T > 0$ is unique up to an additive constant.^{9,10} In inverse statistical-mechanics settings, where the goal is to deduce pair potentials from pair statistics, the theorem is often cited to validate either the proposed inverse methods or the effective pair potentials found.^{11–13}

However, there exist several issues pertaining to fundamental aspects and the practicality of Henderson's theorem. First, the

theorem breaks down at zero and infinite temperatures. The original paper by Henderson claims that the theorem also holds for $T = 0$, but this cannot be true for classical ground states, since it is well known that there exist infinitely many different potential functions consistent with the same ground-state configuration.^{2,14} Indeed, the existence of “universal optimality” of certain lattices rigorously proves this statement.¹⁵ Different potentials could also exhibit similar sequences of ground-state crystal phases as the density varies.¹⁶ At positive but finite temperatures, Henderson's theorem holds rigorously, but its practical effectiveness is an open question, since the sensitivity of pair statistics on pair potentials is not known *a priori*, i.e., the functional derivative $\delta g_2/\delta v$ or $\delta S/\delta v$. For the potential to be uniquely determined, $g_2(r)$ or $S(k)$ must be known exactly and over an infinite range, which is never achieved in experiments or computer simulations.¹⁷ However, to our knowledge, the aforementioned sensitivity has not been quantitatively scrutinized to any

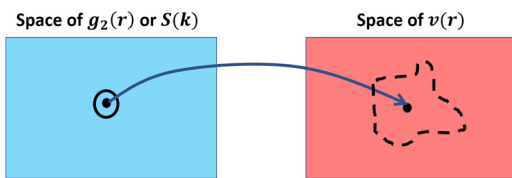


FIG. 1. At $0 < T < \infty$, Henderson's theorem is not practically applicable if very similar pair correlation functions correspond to distinctly different pair potentials.

large degree, and its dependence on the density and temperature has not yet been studied.

In this work, we focus on the practical utility of Henderson's theorem (Fig. 1). This interesting question was raised as an unsolved problem by Potestio.¹⁸ Based on sensitivity metrics that we introduce here, we show that we can devise very different potentials whose corresponding pair statistics $g_2(r)$ and/or $S(k)$ are similar within typical numerical or experimental errors up to some maximum value of r or k , respectively, typically measured in practice. The cases that we identified include ordered and disordered phases at various densities and temperatures. Our findings imply that it is insufficient to use Henderson's theorem alone to claim the uniqueness of effective pair potentials found in practice. Thus, our work has implications for the common and important practice of ascertaining effective pair interactions of complex many-body systems from their pair statistics alone.^{4,6,17,19–33}

In Sec. II, we provide basic definitions, including those for pair statistics, and sensitivity metrics that measure the variation in the pair statistics associated with any given variation in the corresponding pair potential. In Sec. III, we describe the numerical methodologies that we have designed to identify cases in which different potentials give similar pair statistics, as measured by the sensitivity metrics. In Sec. IV, we present examples in fluid and crystal phases as well as unusual low-temperature disordered states in two dimensions (2D), all of which possess low sensitivity metrics, thus demonstrating the practical shortcomings of Henderson's theorem. Specifically, at temperatures above freezing or condensation temperatures, but far below the infinite-temperature limit [where $g_2(r)$ is identically unity], we identified low-density fluids where $S(k)$'s are insensitive to variations of $v(r)$ and high-density fluids where $g_2(r)$'s are insensitive. Such insensitivity also applies to certain crystals at T below half of the melting temperature. We also report a case that we have discovered in which a liquid and a disordered low-temperature state below the melting temperature have similar pair statistics. In Sec. V, we study the dependence of this sensitivity on the density, temperature, and dimensionality. In Sec. VII, we generalize Henderson's theorem by extending the uniqueness statement to potentials that involve two- and higher-body interactions. We make concluding remarks in Sec. VIII.

II. DEFINITIONS AND PRELIMINARIES

In this section, we introduce some fundamental concepts in statistical mechanics of classical many-body systems. Then, we define metrics that quantify differences in potentials and pair statistics, as well as the sensitivity of pair statistics on pair potentials.

A. Pair statistics

We study many-particle systems in d -dimensional Euclidean space \mathbb{R}^d , which completely statistically characterized by the n -particle probability density functions $\rho_n(\mathbf{r}_1, \dots, \mathbf{r}_n)$ for all $n \geq 1$. In the case of statistically homogeneous systems, $\rho_1(\mathbf{r}_1) = \rho$ and $\rho_2(\mathbf{r}_1, \mathbf{r}_2) = \rho^2 g_2(\mathbf{r})$, where $\mathbf{r} = \mathbf{r}_2 - \mathbf{r}_1$ and $g_2(\mathbf{r})$ is the pair correlation function. If the system is in addition statistically isotropic, $g_2(\mathbf{r}) = g_2(r)$, where $r = \|\mathbf{r}\|$. The ensemble-averaged structure factor $S(\mathbf{k})$ is defined as

$$S(\mathbf{k}) = 1 + \rho \tilde{h}(\mathbf{k}), \quad (1)$$

where $h(\mathbf{r}) = g_2(\mathbf{r}) - 1$ is the total correlation function and $\tilde{h}(\mathbf{k})$ is the Fourier transform of $h(\mathbf{r})$.

For a single periodic configuration containing N point particles at positions $\mathbf{r}^N = (\mathbf{r}_1, \mathbf{r}_2, \dots, \mathbf{r}_N)$ within a fundamental cell F of a lattice Λ , the scattering intensity $\mathcal{S}(\mathbf{k})$ is defined as

$$\mathcal{S}(\mathbf{k}) = \frac{\left| \sum_{i=1}^N e^{-i\mathbf{k} \cdot \mathbf{r}_i} \right|^2}{N}. \quad (2)$$

For an ensemble of periodic configurations of N particles within the fundamental cell F , the ensemble average of the scattering intensity in the infinite-volume limit is directly related to the structure factor $S(\mathbf{k})$ by

$$\lim_{N, V_F \rightarrow \infty} \langle \mathcal{S}(\mathbf{k}) \rangle = (2\pi)^d \rho \delta(\mathbf{k}) + S(\mathbf{k}), \quad (3)$$

where V_F is the volume of the fundamental cell and δ is the Dirac delta function.³⁴ In simulations of many-body systems with finite N under periodic boundary conditions, Eq. (2) is used to compute $S(\mathbf{k})$ directly by averaging over configurations.

B. Distance and sensitivity metrics

Here, we first define metrics that quantify “distances” between functions associated with pair statistics and pair potentials. Based on these quantities, we then define sensitivity metrics that measure the variation in pair statistics associated with any given variation in the corresponding pair potentials.

Let $v^{(0)}(r)$, $v^{(1)}(r)$ be stable pairwise additive radial potentials whose Fourier transforms in \mathbb{R}^d exist,³⁵ $g_2^{(0)}(r)$, $g_2^{(1)}(r)$ be the corresponding radial distribution functions at given ρ , T , and $S^{(0)}(k)$, $S^{(1)}(k)$ be the corresponding structure factors. We define the “distance” between v_0 and v_1 as

$$D_v(v^{(0)}, v^{(1)}) = \int_{\mathbb{R}^d} \left[\exp(-v^{(0)}(\mathbf{r})) - \exp(-v^{(1)}(\mathbf{r})) \right]^2 d\mathbf{r}, \quad (4)$$

where D_v is equivalent to the L_2 -norm of the difference in the Mayer functions $y(\mathbf{r}) = \exp(-v(\mathbf{r})/k_B T) - 1$ at $k_B T = 1$ and gives a norm to the space of pair potentials. The exponential transformation in Eq. (4) ensures that D_v is bounded for stable and square integrable potentials. Similarly, the “distance” in the Fourier transforms \tilde{v} of the potentials is defined as

$$\begin{aligned} D_{\tilde{v}}(\tilde{v}^{(0)}, \tilde{v}^{(1)}) &= \int_{\mathbb{R}^d} [\tilde{y}^{(0)}(\mathbf{k}) - \tilde{y}^{(1)}(\mathbf{k})]^2 d\mathbf{k} \\ &= (2\pi)^d D_v(v^{(0)}, v^{(1)}), \end{aligned} \quad (5)$$

where \tilde{y} is the Fourier transform of y . The “distance” between pair statistics D_f is defined as the L_2 -norm,

$$D_f(f^{(0)}, f^{(1)}) = \int_{\mathbb{R}^d} [f^{(0)}(\mathbf{x}) - f^{(1)}(\mathbf{x})]^2 d\mathbf{x}, \quad (6)$$

where $f(x)$ is $g_2(r)$ or $S(k)$. The metric D_f is defined only for systems at positive temperatures since it diverges for two ground states of different crystal structures. Finally, the sensitivity metrics of pair statistics on pair potentials for systems (0) and (1) are defined as

$$C_{g_2}^{0,1} = \frac{D_{g_2}(g_2^{(0)}, g_2^{(1)})}{D_v(v^{(0)}, v^{(1)})} = \frac{\int_{\mathbb{R}^d} [\tilde{h}^{(0)}(\mathbf{k}) - \tilde{h}^{(1)}(\mathbf{k})]^2 d\mathbf{k}}{D_{\tilde{v}}(\tilde{v}^{(0)}, \tilde{v}^{(1)})}, \quad (7)$$

$$C_S^{0,1} = \frac{D_S(S^{(0)}, S^{(1)})}{D_{\tilde{v}}(\tilde{v}^{(0)}, \tilde{v}^{(1)})} = \rho^2 C_{g_2}^{0,1}. \quad (8)$$

If the systems in question are clear from the context, the superscripts (0) and (1) can be omitted. We note that the state $\rho = 0$, $k_B T = 1$ can be thought of as a reference state, as C_{g_2} is unity for any pair of potentials. We consider systems to be of low sensitivity if C_{g_2} and C_S are smaller than 0.005 and high sensitivity if they are greater than 1.

We remark here that one could employ other metrics to analyze the relationship between pair statistics and pair potentials. A commonly used metric is the Jensen–Shannon divergence between two systems.³⁶ It is defined as

$$D_{JS} = \frac{-\rho^2}{2k_B T} \int_{\mathbb{R}^d} [v^{(0)}(\mathbf{r}) - v^{(1)}(\mathbf{r})] [g_2^{(0)}(\mathbf{r}) - g_2^{(1)}(\mathbf{r})] d\mathbf{r}. \quad (9)$$

In fact, $D_{JS} = D_{0,1} + D_{1,0}$, where $D_{i,j}$ is the relative entropy (or the Kullback–Leibler divergence) of system i with respect to system j . The relative entropy is a natural metric of the “distance” in probability distributions and arises in the proof of Henderson’s theorem. It does not directly measure distances in pair statistics or pair potentials but is rather a mixture of the two, and hence, we do not consider this metric in our work.

In this work, unless otherwise stated, systems labeled with (0) are called target systems, i.e., systems whose pair statistics are to be reconstructed via inverse methods. Systems labeled with (1) are called inferred systems, i.e., they are solutions to inverse problems targeting $g_2^{(0)}(r)$ or $S^{(0)}(k)$.

C. Common pair potentials

This subsection defines a variety of common potentials used in this work. The generalized Lennard-Jones (LJ) potential v_{LJ} is defined as

$$v_{LJ}(r; \sigma, \epsilon, a, b) = \epsilon \left[\left(\frac{\sigma}{r} \right)^a - \left(\frac{\sigma}{r} \right)^b \right], \quad (10)$$

where $\sigma > 0$, $\epsilon > 0$, and $a > b > 0$. The power-law (PL) repulsive potential is defined as

$$v_{PL}(r; \sigma, \epsilon, a) = \epsilon \left(\frac{\sigma}{r} \right)^a, \quad (11)$$

where $\sigma > 0$, $\epsilon > 0$, and $a > 0$. The Gaussian-core (GC) potential is defined as

$$v_{GC}(r; \sigma, A) = A \exp \left(-\frac{r^2}{\sigma^2} \right), \quad (12)$$

where $\sigma > 0$ and $A > 0$.

The “overlap” potential is defined as³⁷

$$v_{overlap}(r; V_0, K) = \frac{V_0}{\pi(Kr)^2} \left[J_1 \left(\frac{Kr}{2} \right) \right]^2, \quad (13)$$

where $V_0 > 0$, $K > 0$, and J_1 is the first-order Bessel function. The Fourier transform of $v_{overlap}(r)$ yields the overlapping area of two 2D disks whose centers are separated by a certain distance. The “overlap” potential is reminiscent of the effective interaction used to model multilayered ionic micogels.³⁸ Finally, a potential used to model the effective pair interactions of “star” polymers³⁹ is given by

$$\begin{aligned} v_{star}(r; \sigma, f) &= \begin{cases} \frac{5}{18} f^{\frac{3}{2}} \left[-\ln \left(\frac{r}{\sigma} \right) + \left(1 + \frac{\sqrt{f}}{2} \right)^{-1} \right], & r \leq \sigma \\ \frac{5}{18} f^{\frac{3}{2}} \left(1 + \frac{\sqrt{f}}{2} \right)^{-1} \left(\frac{r}{\sigma} \right)^{-1} \exp \left[-\frac{\sqrt{f}}{2} \left(\frac{r}{\sigma} - 1 \right) \right], & r > \sigma, \end{cases} \end{aligned} \quad (14)$$

where $\sigma > 0$ and $f > 0$ is the number of branches on a polymer particle.

We selected these potentials due to their variety of interaction ranges, repulsion steepness, monotonicity, or minima positions and available phases. The LJ and power-law potentials are short-ranged hard-core potentials that diverge as $r \rightarrow 0$. The Gaussian core and the “star” potentials are bounded and have been used to model polymers. The “overlap” potential is a long-ranged, bounded potential that exhibits unusual disordered ground states at certain densities.³⁷

D. Inverse algorithms

In this subsection, we briefly describe some inverse-problem concepts and algorithms that we will employ in Sec. III to identify cases of low sensitivity metrics. We consider the class of inverse problems where the goal is to deduce effective pair potentials consistent with some given target pair statistics $f^*(x)$.^{2,40}

We begin by summarizing a general inverse procedure that encompasses previous methodologies. Let U be the space of all stable and square integrable pair potentials on \mathbb{R}^d whose Fourier transforms exist. An inverse procedure usually follows an iterative process that starts with an initial trial potential $v_{t,0} \in U$. A Monte Carlo simulation of a many-body system is performed under $v_{t,0}$ to obtain an ensemble of equilibrium configurations, from which the trial pair statistics $f_{t,0}(\mathbf{x})$ are computed. Specifically, $g_2(\mathbf{r})$ is computed from an ensemble-averaged pair distance histogram, and $S(\mathbf{k})$ is computed

from the ensemble-averaged scattering intensity [Eq. (2)]. The process terminates if $f_{t,i}$ is deemed close to the target f^* , i.e., $D_f(f_{t,i}, f^*) \leq \epsilon$ for some tolerance ϵ on the order of experimental or simulation errors. If not, an algorithm-specific functional $F: U \rightarrow U$, called updating rule, maps $v_{t,0}$ to an improved trial potential $v_{t,1}$ by taking into account the difference between $f_{t,0}$ and f^* . This process iterates until it finds a trial potential $v_{t,i}$ in the i th iteration such that $D_f(f_{t,i}, f^*) \leq \epsilon$. The potential $v_{t,i}$ is then considered a solution to the inverse problem. Figure 2 illustrates the general inverse procedure described above.

There are various algorithms implementing the general procedure described above. They differ in their updating rules and requirements for trial potentials.^{19–21,27,31–33} Algorithms applied in this work are Iterative Boltzmann Inversion (IBI)²¹ and gradient descent optimization, chosen because of their generality and implementation simplicity. IBI uses unparameterized potentials and has a point-by-point updating rule,

$$v_{t,i+1}(\mathbf{r}) = v_{t,i}(\mathbf{r}) + \lambda \ln\left(\frac{g_2^{t,i}(\mathbf{r})}{g_2^*(\mathbf{r})}\right), \quad (15)$$

where $\lambda > 0$ is a tunable “step size” parameter. The initial trial potential $v_{t,0}$ for IBI is usually the potential of mean force (PMF) corresponding to the target pair correlation function, given by²¹

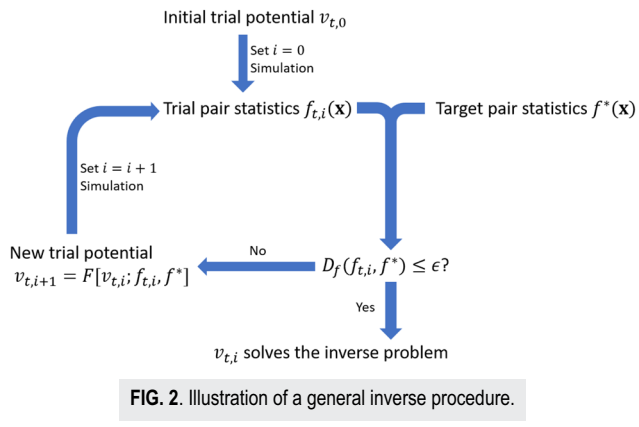
$$v_{\text{PMF}}(\mathbf{r}) = -k_B T \ln(g_2^*(\mathbf{r})). \quad (16)$$

IBI is a general algorithm that has been used to study inverse problems of disordered phases.⁴¹ However, for crystal phases, the trial potentials may fail to converge because Eq. (15) always generates long-ranged trial potentials for long-range correlations. Therefore, when targeting crystal $g_2(r)$'s, the trial potentials contain many unphysical deep minima.

Gradient descent optimization uses parameterized trial potentials $v_{t,i}(\mathbf{r}; \mathbf{a}_i)$, where \mathbf{a}_i is the vector of potential parameters. The parameters are updated in each iteration by the rule

$$\mathbf{a}_{i+1} = \mathbf{a}_i - \mu \nabla D_f(f^*, f_{t,i}), \quad (17)$$

where $\mu > 0$ is the “step size” parameter. Implementation details for both algorithms will be given in Sec. III.



III. METHODOLOGY

In this section, we describe our methods to identify low-sensitivity cases, i.e., examples in which C_{g_2} and/or C_S have potentially low values. Finding such cases would demonstrate practical shortcomings of Henderson's theorem. In this section and Sec. IV, we restrict our attention to stable, square integrable, and isotropic pair potentials on \mathbb{R}^2 whose Fourier transforms exist.

A. Setup of the inverse problem

Let $v_0(r)$ be a known pair potential for the target system, with corresponding pair statistics $g_2^{(0)}(r)$ or $S^{(0)}(k)$ at ρ, T . We aim to find an inferred pair potential $v_1(r)$ with pair statistics $g_2^{(1)}(r)$ and $S^{(1)}(k)$ such that the distance metric between $v_0(r)$ and $v_1(r)$ is large, whereas the distance metrics between the target and inferred $g_2(r)$'s and/or $S(k)$'s are comparable to typical errors in experiments or simulations up to ranges typically measured, defined more precisely below. To do this, we implemented inverse algorithms that target $g_2^{(0)}(r)$, as described in Sec. II D. IBI was used to target disordered states, and gradient descent optimization was used for crystals states. Note that we did not directly target $S^{(0)}(k)$ “on the fly” due to the lack of a general Fourier-based inverse algorithm. Instead, whenever a small C_S is prescribed, we applied Eq. (1) to obtain $g_2^{(0)}(r)$ from the targeted $S^{(0)}(k)$.

B. Maximizing the potential-distance metric between target and inferred potentials

Ideally, for any prescribed D_{g_2} or D_S , it is desirable to find the potential $v_1(r)$ such that the distance metric between the target and inferred potentials is maximized. However, due to the computational challenge of this task, we instead attempted to identify inferred potentials that yield low sensitivity metrics. To do this, we required that the trial potentials $v_{t,i}(r)$ possess distinct features from $v_0(r)$ in terms of monotonicity, steepness of repulsive forces, and positions of minima/maxima. Therefore, in gradient descent optimization, the parameterized trial potentials were constrained to functional forms different from $v_0(r)$. For example, if $v_0(r)$ is a power-law potential, $v_{t,i}(r)$ were set to be LJ potentials. For IBI, since the trial potentials are not parameterized, we set the initial guess potential $v_{t,0}(r)$ to be distinct from $v_0(r)$ in the aforementioned senses. Examples are given in Sec. IV A.

In some instances, to further increase the difference between $v_0(r)$ and $v_1(r)$, we added a small perturbing function $p(r)$ or $\tilde{p}(k)$ to $g_2^{(0)}$ or $S^{(0)}(k)$ and set the perturbed pair statistics as the target of the inverse procedure. The L_2 -norm of the perturbing function was smaller than that caused by typical experimental errors. Exact expressions of the perturbing functions we used will be given in Sec. IV.

C. Computation of sensitivity metrics

Since we focus on practical aspects of Henderson's theorem, we select ranges of pair statistics typically measured in simulations or experiments and commonly used as targets for practical inverse problems. To compute the distance metrics defined in Eqs. (4)–(6), we cut off the integration at $r = 8$ in direct space and

$k = 20$ in Fourier space. The definitions of the unit length depend on the potentials [e.g., the parameter σ for $v_{\text{LJ}}(r)$], but in all cases, we note that the first peaks of $g_2(r)$ are in the range $0.5 \leq r \leq 2.0$. We computed C_S directly by both $D_S/D_{\tilde{v}}$ and $\rho^2 C_{g_2}$ and found that they agreed with each other very well (relative error <0.5%) except for crystal phases, indicating that the ranges that we used to compute Eqs. (4)–(6) are large enough to approximate the integrations over infinite volume.

D. Simulations of trial potentials and stopping criteria

In our implementation of inverse algorithms, the trial pair correlation functions $g_2^{t,i}(r)$ were obtained from Monte Carlo simulations with 400 particles for fluids or 418 particles for crystals in the triangle lattice arrangement in 2D under periodic boundary conditions, averaged over 200 equilibrium configurations. We chose suitable stopping criteria to be those determined by typical experimental errors in pair statistics, which we quantified as a root mean square error (RMSE) of 0.03 for both $g_2(r)$ and $S(k)$.⁴² Up to the ranges specified in Sec. III C, this RMSE corresponds to $D_{g_2} = 0.18$, $D_S = 1.1$ in 2D. Our stopping criteria were $D_{g_2}(g_2^{(0)}, g_2^{t,i}) \leq 0.05$ for IBI and $D_{g_2}(g_2^{(0)}, g_2^{t,i}) \leq 0.10$ for gradient descent optimization. The former criterion is comparable to random errors of these simulations. The latter criterion is more relaxed because there are fewer degrees of freedom to optimize for parameterized potentials, and precision up to simulation errors often cannot be achieved. However, both criteria are much more stringent than the typical experimental errors just defined.

E. Large-scale simulations

After an appropriate potential v_1 was found by inverse algorithms, we carried out large-scale simulations to obtain highly precise pair statistics, as reported. Monte Carlo simulations were performed for 1000 particles for fluids or 1020 particles for crystals in the triangle lattice arrangement in 2D (Secs. IV and V) and 4000 particles in 3D (Sec. V in the discussion of dimensionality) under periodic boundary conditions, averaged over 500 equilibrium configurations. These simulations are able to achieve random error $D_{g_2} \leq 0.01$.

IV. EXAMPLES THAT YIELD LOW SENSITIVITY METRICS

In this section, we focus our attention to the potentials defined in Sec. II C and present various states of matter that yield low sensitivity metrics C_{g_2} and/or C_S . These include fluids at high and low densities, crystals, and unusual disordered low-temperature states.

A. High-density fluids

High-density fluids include liquids and supercritical fluids with liquid-like densities. For these states, short-range interactions dictate much of the pair statistics. In Fig. 3, we show an example, at $\rho = 1.29$, $k_B T = 4$, where widely different pair potentials produce similar $g_2(r)$ [Figs. 3(a) and 3(b)]. The potential v_0 is defined by $v_0(r) = v_{\text{overlap}}(r; 1000, 7.6634)$ [Eq. (13)]. This choice of parameters sets the unit length at the first minimum of $v_0(r)$. The potential $v_1(r)$

was obtained by IBI targeting $g_2^{(0)}(r)$, where the initial guess potential was $v_{\text{GC}}(r; 100, 1)$ [Eq. (12)], deliberately set to have a much larger repulsive range than v_0 . As seen from Fig. 3(a), the apparent distinction in the pair potentials affects the tail of $g_2(r)$ only slightly, but in Fourier space, the difference is manifest in the small k behavior of the structure factor [Fig. 3(c)]. The red-dashed curve in Fig. 3(b) shows that $v_1(r) - 5.0$ agrees very well with $v_0(r)$ for $r < 1$. Therefore, in this example, v_1 captures the interparticle forces, i.e., the steepness of v_0 in the small r range, but intermediate- to long-range interactions were not well captured.

Zhang and Torquato⁴³ developed a relation between the structure factor and the Fourier transform of the potential $\tilde{v}(k)$, provided that the \mathbf{k} -vectors were independent,

$$\tilde{v}(k) = k_B T \left(\frac{1}{S(k)} - 1 \right), \quad (18)$$

which is exact in the infinite density limit. Indeed, we found that Eq. (18) is already a good approximation for liquid densities. Taking derivative of $\tilde{v}(k)$ with respect to $S(k)$ while fixing k , we have

$$\frac{\delta \tilde{v}(k)}{\delta S(k)} = -k_B T \frac{1}{(S(k))^2}. \quad (19)$$

It is, therefore, predicted that for high-density fluids, the pair potential is sensitive to variations in $S(k)$ where the latter has small values. In practice, we found that perturbing at regions of k where $S(k) \leq 0.01$ suffices to exhibit this effect. Figure 4 shows an example at $\rho = 0.75$, $k_B T = 0.58$, where $v_0(r) = v_{\text{LJ}}(r; 1, 4, 6, 12)$ and $v_1(r)$ was obtained by IBI targeting $g_2(r)$ corresponding to a perturbed structure factor $S^*(k) = S^{(0)}(k) + \tilde{p}(k)$. The perturbing function is given by

$$\tilde{p}(k) = \begin{cases} 0, & k \leq a \\ \frac{A \sin\left(2\pi w \frac{k-a}{b-a}\right)}{2\pi k}, & a < k < b \\ 0, & k \geq b, \end{cases} \quad (20)$$

where we set $A = -0.3$, $a = 0.1$, $b = 5$, and $w = 1$. The initial trial potential was obtained by Eq. (18). It can be seen from Figs. 4(a) and 4(c) that comparing the target and inferred systems, both the pair of $g_2(r)$'s and the pair of $S(k)$'s agree very well, even though the pair potentials have their minima at completely different r , and their repulsive parts are in no way similar [Fig. 4(b)]. Indeed, the inset of Fig. 4(b) shows that the forces derived from the target and inferred potentials are significantly different for interparticle distances in the vicinity of the first peak of $g_2(r)$. It is reasonable to assume that due to an effective hard core in both potentials, steric constraints on local packing configurations play a more important role in determining the pair statistics than the precise forms of the intermolecular forces.

The low sensitivity of $g_2(r)$ on pair potentials for high-density fluids dominated by steep short-range repulsive interactions is expected from the modern liquid-state theory, where it is known that away from the critical point, the local structure of a fluid is primarily determined by steric effects caused by the repulsive

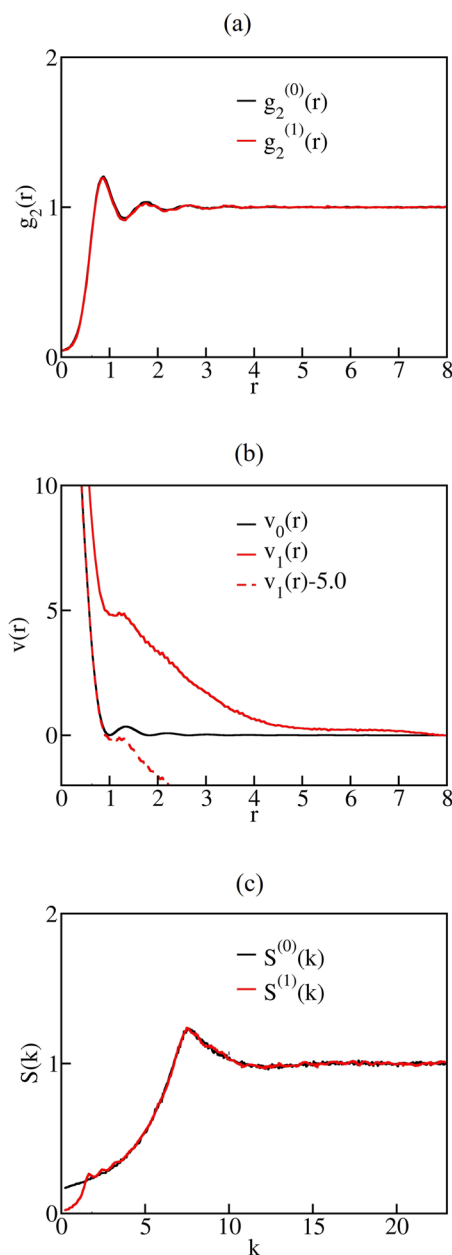


FIG. 3. (a) Pair correlation functions of two high-density fluids, where $g_2^{(0)}(r)$ was set as the target to obtain the inferred system. (b) Black solid: $v_0(r) = v_{\text{overlap}}(r; 1000, 7.6634)$; red solid: v_1 obtained by IBI with the initial guess $v_{\text{GC}}(r; 100, 1)$, targeting $g_2^{(0)}(r)$. Red dashed: $v_1(r) - 5.0$. (c) Structure factors of the fluids. $\rho = 1.29$, $k_B T = 4$, $T \approx 6.0T_{\text{freeze}}^{(0)} \approx 6.0T_{\text{freeze}}^{(1)}$. $D_v = 35.3$, $D_{g_2} = 3.7 \times 10^{-3}$, $D_s = 0.24$. $C_{g_2} = 1.0 \times 10^{-4}$, $C_s = 1.7 \times 10^{-4}$.

forces.^{44,45} Indeed, using different parameterizations in Empirical Potential Structure Refinement (EPSR), Soper found various pair potentials that reconstruct the pair statistics of a LJ fluid reasonably well.²³ Several other studies have also noticed the propensity of

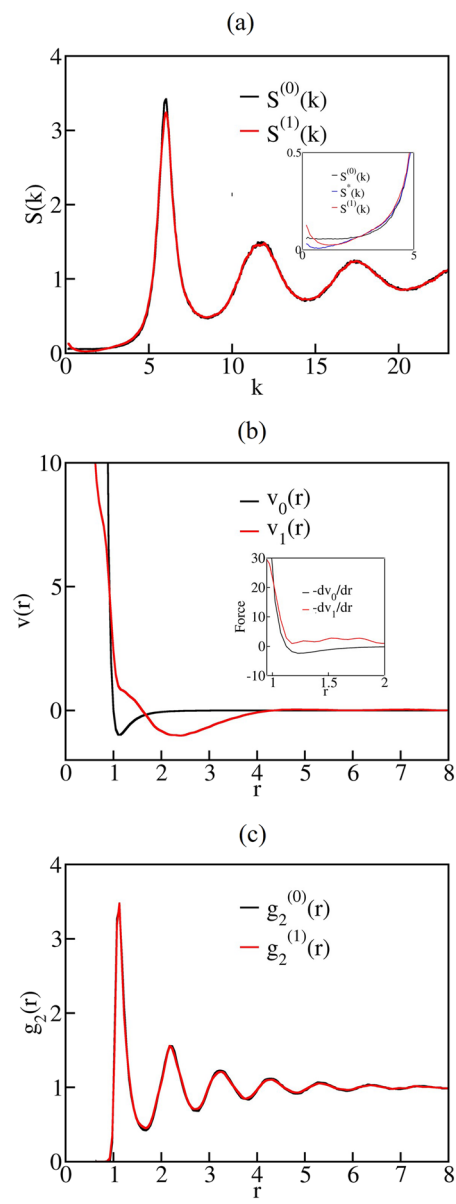


FIG. 4. (a) Structure factors of two high-density fluids, where a slightly perturbed $S^{(0)}(k)$, namely, $S^*(k)$, was set as the target to obtain the inferred system. (b) Black solid: $v_0(r) = v_{\text{LJ}}(r; 1, 4, 6, 12)$; red solid: v_1 generated using IBI targeting $g_2(r)$ corresponding to the perturbed $S^{(0)}(k)$. Inset: Forces generated by the target and inferred potentials. (c) Pair correlation functions of the fluids. $\rho = 0.75$, $k_B T = 0.58$, $T \approx 1.4T_{\text{freeze}}^{(0)} \approx 1.2T_{\text{freeze}}^{(1)}$. $D_v = 50.5$, $D_{g_2} = 0.050$, $D_s = 1.1$, $C_{g_2} = 9.9 \times 10^{-4}$, $C_s = 5.6 \times 10^{-4}$.

IBI, which targets $g_2(r)$ only, to arrive at potentials different from the true ones while reproducing the target $g_2(r)$ within numerical errors.^{32,46–48} This effective nonuniqueness has inspired studies to improve on the standard IBI procedure such that the derived

effective pair potentials can reproduce thermodynamic properties at multiple state points.^{49,50} Still, we believe that the examples in Figs. 3 and 4 are the most compelling illustrations of this low sensitivity so far. Furthermore, Fig. 4 clearly shows that even short-ranged repulsive forces can be difficult to reproduce by inverse procedures. These examples imply that in inverse problems for high-density fluids, $S(k)$ or other long-range information must be incorporated into the target, and extremely precise structure factor data must be provided where $S(k)$ is small.

B. Low-density fluids

Due to the relation, Eq. (1), at low densities, a small perturbation in $S(k)$ at large k could lead to large variations in $g_2(r)$ at small r , and conversely, perturbations of $S(k)$ at small k affect the large- r behaviors of $g_2(r)$. The variations in $g_2(r)$'s, in turn, could imply significant differences in the corresponding pair potentials according to Eq. (16).

Figure 5 shows an example at $\rho = 0.05$, $k_B T = 1$, where the pair of $S(k)$'s are similar, whereas the pair of $g_2(r)$'s are distinctly different in so far as small- r behaviors are considered. Both potentials were found by IBI. The potential $v_0(r)$ was obtained by targeting a predefined pair correlation function $g_2^{*(0)}(r)$, given by

$$g_2^{*(0)}(r) = \max(g_2^{\text{star}}(r), 0.2), \quad (21)$$

where $g_2^{\text{star}}(r)$ is the pair correlation function corresponding to the “star” potential $v_{\text{star}}(r; 1, 18)$ [Eq. (14)]. The potential $v_1(r)$ was obtained by targeting the pair correlation function corresponding to a perturbed $S^{(0)}(k)$. The perturbing function $\tilde{p}(k)$ is given by Eq. (20) with $A = 1$, $a = 15$, $b = 20$, and $w = 2$. We chose such $\tilde{p}(k)$ to mimic the effect of small uncertainties in real data in the tail of $S(k)$. As we can see in Fig. 5(a), the difference in the structure factors is only slightly noticeable in the tail region where $S^{(0)}(k)$ is identically unity. However, as shown in Figs. 5(b) and 5(c), the functions $v_1(r)$ and $g_2^{(1)}(r)$ for the inferred system possess high-frequency oscillations that are not observed for the target system. Importantly, this example demonstrates the ambiguity of solutions to inverse problems targeting pair statistics over a finite range: Since $S^{(0)}(k)$ and $S^{(1)}(k)$ are almost identical for $k < 15$, an inverse procedure that targets $S^{(1)}(k)$ only for the range $k < 15$ will not be able to reconstruct the high-frequency oscillations in $v_1(r)$. We remark that potentials like $v_1(r)$ are unlikely to be found in laboratory, but we mathematically demonstrate that $S(k)$ can be insensitive to the pair potential at low densities. We also note that $S(k)$'s at low densities can be well approximated by the Baxter model, where the second-virial coefficients are similar for different potentials.²⁸

C. Crystals

“Universal optimality” mentioned in the Introduction establishes that many pair potentials share the same ground state crystal configuration. For the same lattice at a positive temperature (but below melting), the pair statistics is dictated by phonon behaviors.

Figure 6 shows two triangle lattice states at $\rho = 1.15$, $k_B T = 0.1$, where $v_0(r) = v_{\text{PL}}(r; 1, 3.77, 4)$ [Eq. (11)] and $v_1(r) = v_{\text{LJ}}(r; 1, 9.2, 4, 3)$

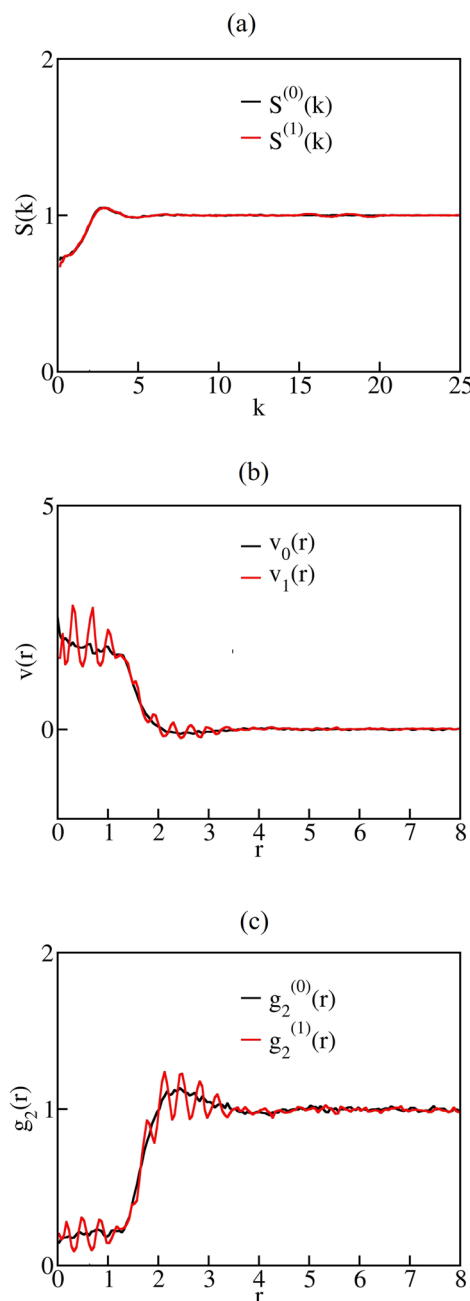


FIG. 5. (a) Structure factors of two low-density fluids, where a slightly perturbed $S^{(0)}(k)$ was set as the target to obtain the inferred system. (b) Two potentials found by IBI, described in Sec. IV B. (c) Pair correlation functions of the fluids. $\rho = 0.05$, $k_B T = 1$, $T \approx 6.7T_{\text{condense}}^{(0)} \approx 6.7T_{\text{condense}}^{(1)}$. $D_v = 0.35$, $D_{g_2} = 0.29$, $D_s = 0.030$, $C_{g_2} = 0.82$, $C_S = 2.0 \times 10^{-3}$.

[Eq. (10)]. $v_1(r)$ is found by gradient descent optimization of the parameter ϵ in $v_{\text{LJ}}(r; 1, \epsilon, 4, 3)$, targeting $g_2^{(0)}(r)$. The temperature is about 0.17 of the melting temperature for $v_0(r)$ at this density. As seen from C_{g_2} and C_S , the sensitivity of pair statistics on pair

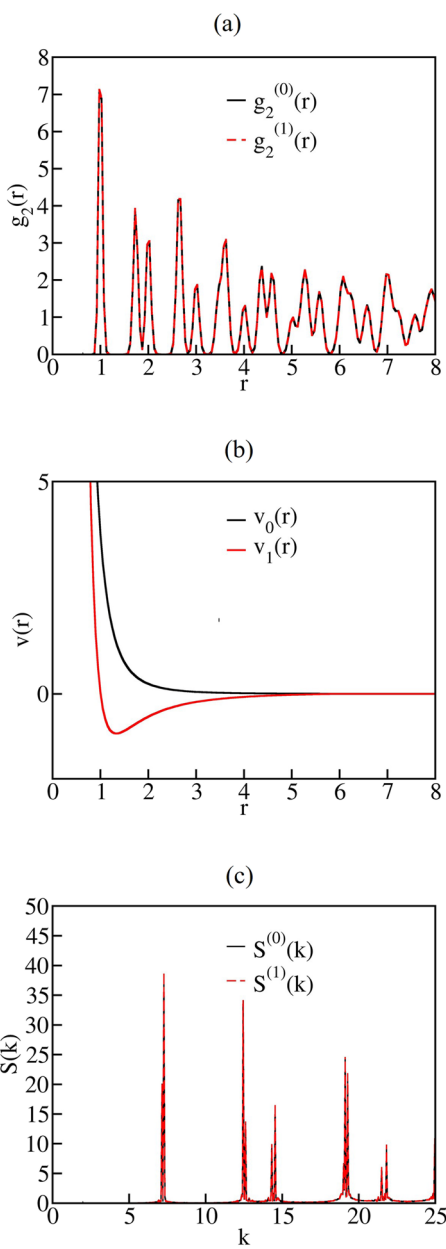


FIG. 6. (a) Pair correlation functions of two crystals adopting the triangle lattice structure, where $g_2^{(0)}(r)$ was set as the target to obtain the inferred system. (b) Black solid: $v_0(r) = v_{PL}(r; 1, 3.77, 4)$; red solid: $v_1(r) = v_{LJ}(r; 1, 9.2, 4, 3)$. (c) Structure factors of the two crystals. $\rho = 1.15, k_B T = 0.1, T \approx 0.17T_{\text{melting}}^{(0)} \approx 0.17T_{\text{melting}}^{(1)}$. $D_v = 36, D_{g_2} = 0.011, D_S = 2.3, C_{g_2} = 3.1 \times 10^{-4}, C_S = 1.6 \times 10^{-3}$.

potential is extremely low. D_S in Fig. 6(c) is large due to the very high peaks, but the percentage difference of peak height is smaller than 0.2%. We will see in Sec. V that the sensitivity metrics of these two potentials are low for a wide range of densities and temperatures.

Also, note that the relation $C_S = \rho^2 C_{g_2}$ does not hold in this case because the cutoff $r = 8$ is too small compared to the range required to approximate the volume integration in the Fourier transform of $h(r)$.

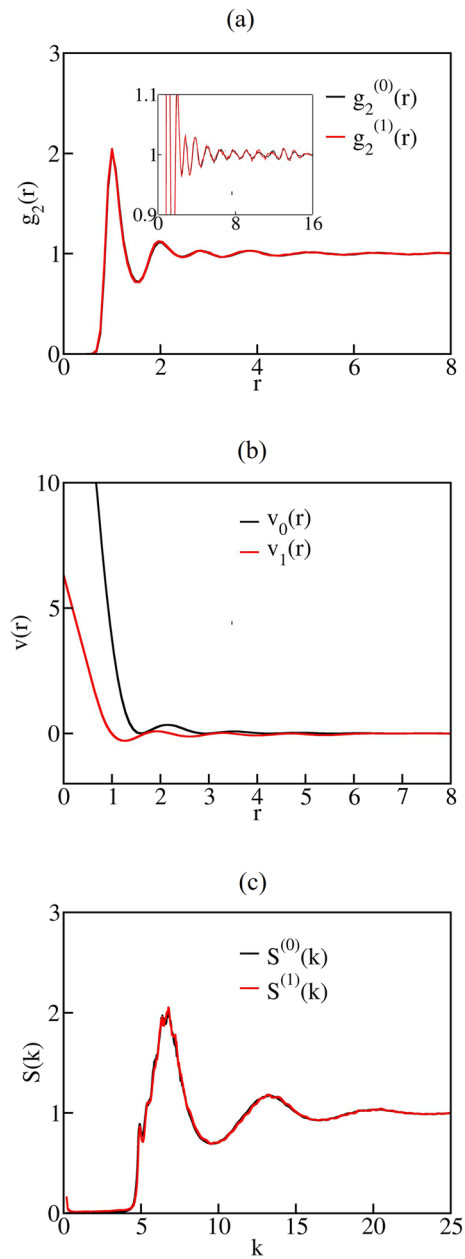


FIG. 7. (a) Pair correlation functions of a disordered low-temperature state (target) and a liquid state (inferred), where $g_2^{(0)}(r)$ was set as the target to obtain the inferred system. The inset shows the long-range correlations. (b) Black solid: $v_0(r) = v_{overlap}(r; 1000, 4.7896)$; red solid: $v_1(r)$ found by IBL targeting $g_2^{(0)}(r)$. (c) Structure factors of the two systems. The spiky "shoulders" are true features of these $S(k)$'s. $\rho = 0.9766, k_B T = 0.07, D_v = 6.2, D_{g_2} = 6.9 \times 10^{-3}, D_S = 0.35, C_{g_2} = 1.1 \times 10^{-3}, C_S = 1.0 \times 10^{-3}$.

D. Low-temperature disordered states

The “overlap” potential has disordered ground states at certain densities, where $g_2(r)$ and $S(k)$ contain no δ -peaks. These ground states highly degenerate and include lattice structures, although disordered states are entropically favored. Such disordered ground states have the intriguing property of being “stealthy hyperuniform,” i.e., the structure factors vanish at some finite interval $0 < k < K$, and their pair correlation functions closely resemble those of a typical dense liquid.³⁷ At small but positive temperatures, we hypothesize that inverse algorithms targeting such $g_2(r)$ ’s could arrive at liquid-like states instead of the true disordered low-temperature states.

In Fig. 7(b), $v_0(r) = v_{\text{overlap}}(r; 1000, 4.7896)$, which has a disordered ground state at $\rho = 0.9766$. The parameters of v_0 are chosen so that the first peak of $g_2^{(0)}(r)$ occurs at $r = 1.0$. At $k_B T = 0.07$, we used IBI to search for a potential that reconstructs $g_2^{(0)}(r)$, where the initial trial potential was the PMF. The inferred potential, $v_1(r)$, is apparently different from $v_0(r)$ in its minima positions and steepness of repulsion [Fig. 7(b)]. Figure 7(c) shows that $S(k)$ ’s of both systems agree closely except at $k < 0.3$: $S^{(0)}(0) = 0.0018$, whereas $S^{(1)}(0) = 0.16$. The fine-scale features of $S(k)$ are real, and we verified that

they correspond to the highly nontrivial long-range correlations in $g_2(r)$ ’s, as shown in the inset of Fig. 7(a). Although the phase diagram of $v_1(r)$ has not yet been studied, the much higher isothermal compressibility of the inferred system compared to the target system suggests that the former is a fluid state. Furthermore, we verified that $g_2^{(1)}(r)$ continues to change significantly upon cooling below $T = 0.07$ (not shown), whereas $g_2^{(0)}(r)$ stays nearly the same, suggesting that the inferred system shown in Fig. 7 is not near its ground state.

V. EFFECT OF DENSITY, TEMPERATURE, AND DIMENSIONALITY

The density and temperature dependence of the sensitivity metrics, described by Eqs. (7) and (8), is shown in Fig. 8 for the fluids of the two potentials $v_0(r) = 3.77r^{-4}$ and $v_1(r) = 9.2(r^{-4} - r^{-3})$. The curve of $k_B T = 2$ has outliers because of liquid-vapor coexistence for v_1 . The higher temperatures are supercritical. One observes from Fig. 8(a) that at fixed temperature and low to medium densities, C_{g_2} decreases exponentially with ρ . At fixed density, C_{g_2} decreases approximately as $1/T$. We conclude that low sensitivity in $g_2(r)$ is found at high-density, high-temperature states. Physically, high densities force particles to be close to each other and weakens the influence of long-range interactions. High temperatures reduce the difference in Boltzmann factors $\exp(-\Phi/k_B T)$, where Φ is the configurational energy. Figure 8(b) plots C_S with respect to ρ , T . We see that the low sensitivity of $S(k)$ occurs at high temperatures and both low and high densities. Low C_S at low ρ is due to the factor ρ^2 in Eq. (8). We also computed the sensitivity metrics for

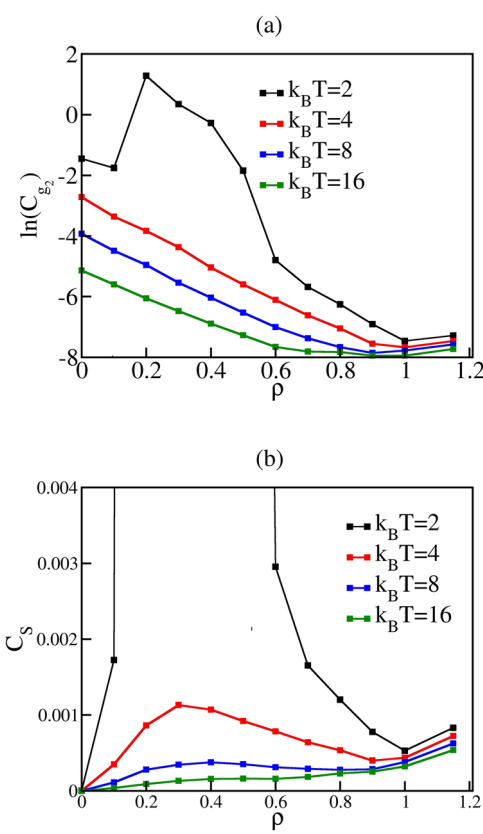


FIG. 8. Plot of the sensitivity metrics for the two potentials $v_0(r) = 3.77r^{-4}$ and $v_1(r) = 9.2(r^{-4} - r^{-3})$. (a) Plot of $\ln C_{g_2}$ against ρ at different T . (b) Plot of C_S against ρ at different T .

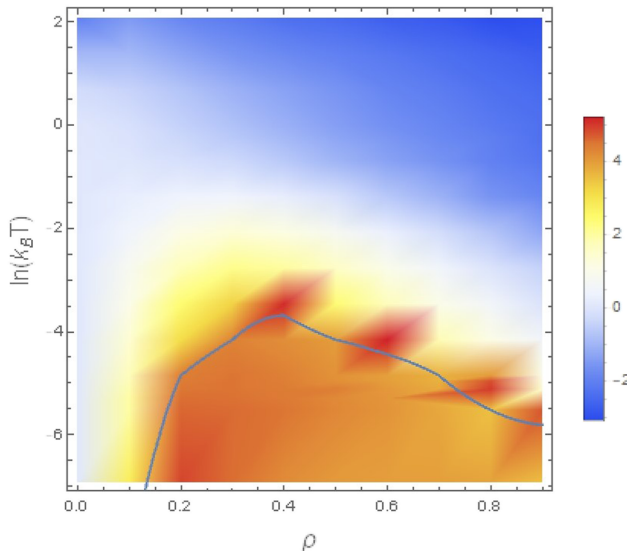


FIG. 9. Plot of $\ln(C_{g_2})$ for the two potentials $v_0(r) = 2 \exp(-r^2)$ and $v_1(r) = 3 \exp(-r^2)$. The blue curve marks the states of solid-fluid phase transition of v_1 . At temperatures slightly above phase transition states, C_{g_2} reaches a maximum at intermediate ρ , corresponding to the structural anomaly observed for the Gaussian core model.

crystals of the same potentials and found that low sensitivity occurs at $T/T_{\text{melting}} < 0.5$.

As another example, we computed C_{g_2} for two Gaussian potentials $v_0(r) = v_{\text{GC}}(r; 2, 1)$ and $v_1(r) = v_{\text{GC}}(r; 3, 1)$ at various

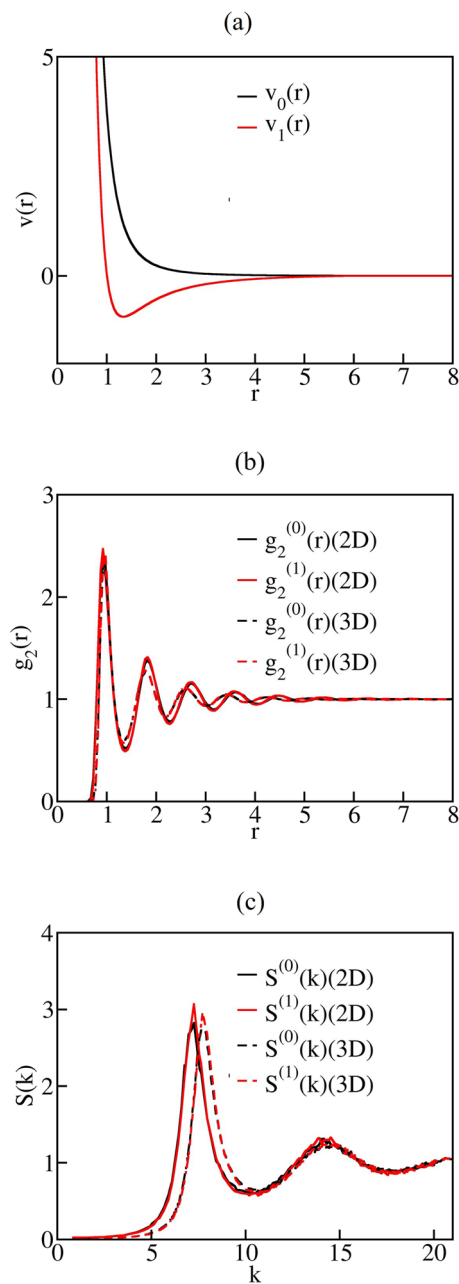


FIG. 10. (a) Black solid: $v_0(r) = v_{\text{PL}}(r; 1, 3.77, 4)$; red dashed: $v_1(r) = v_{\text{LJ}}(r; 1, 9.2, 4, 3)$. (b) Pair correlation functions of v_0 and v_1 in 2D and 3D. (c) Structure factors of v_0 and v_1 in 2D and 3D. For 2D, $\rho = 1.15$, $k_B T = 1.5$, $D_v = 36$, $D_{g_2} = 0.025$, $D_S = 1.3$, $C_{g_2} = 6.9 \times 10^{-4}$, $C_S = 9.2 \times 10^{-4}$. For 3D, $\rho = 1.37$, $k_B T = 0.7$, $D_v = 190$, $D_{g_2} = 0.045$, $D_S = 21$, $C_{g_2} = 2.3 \times 10^{-4}$, $C_S = 4.4 \times 10^{-4}$.

states around solid–fluid phase transition. For temperatures $k_B T/A < 0.011$, the Gaussian core potential in 2D exhibits re-entrant melting upon compression.⁵¹ Figure 9 shows that the sensitivity is highest at phase transition states. For fluids at high enough temperatures, C_{g_2} decreases with density, similar to Fig. 8. However, at lower temperatures such that $T/T_{\text{melting}} < 5$, C_{g_2} reaches a maximum at intermediate densities ($\rho \approx 0.4$). We believe that this is related to the “structural anomaly” observed for the Gaussian core model, i.e., the fluid state at which the entropy reaches a minimum as the density varies.⁵² Unlike the potentials in Fig. 8, these two Gaussian potentials do not generally give low sensitivity in the crystal phase at positive temperatures, although the ground states for both are the triangle lattice.

To demonstrate the effect of dimensionality, we compute sensitivity metrics for potentials in Fig. 6 in both 2D and 3D. In 2D, the state is $\rho = 1.15$, $k_B T = 1.5$, a dense fluid. In 3D, the density and temperature chosen are $\rho = 1.37$, $k_B T = 0.7$. The two states are comparable in terms of heights of the first peaks of $g_2(r)$ and $S(k)$. In fact, assuming the effective particle diameter is 0.925 in 2D and 0.95 in 3D [positions of the first peaks of the corresponding $g_2(r)$'s], $\rho/\rho_{\max} \approx 0.85$ in both the 2D and 3D states, where ρ_{\max} is the density of the densest sphere packing. It can be seen from Fig. 10 that the pair statistics are similar for both 2D and 3D. C_{g_2} and C_S are lower in 3D, probably due to the decorrelation principle in higher dimensions, which results in the faster decay of $g_2(r)$ to unity in 3D.⁵³

VI. DEGENERACY PROBLEM

Although the target and inferred systems presented in Sec. IV have nearly identical $g_2(r)$'s, their higher-order correlation functions can be generally different from one another, which is known as the “structural degeneracy problem.”^{54,55} It has been noted that higher-order correlations play important roles in modeling molecular systems.^{56–58} Therefore, we explore whether any of the target and inferred particle configurations that we have considered have apparently different high-order statistics. We found that the potentials shown in Fig. 7 provide good examples of such instances. Figure 11 shows snapshots of the target and inferred systems that are obtained from the potentials shown in Fig. 7. Compared to the inferred system, the target system has smaller

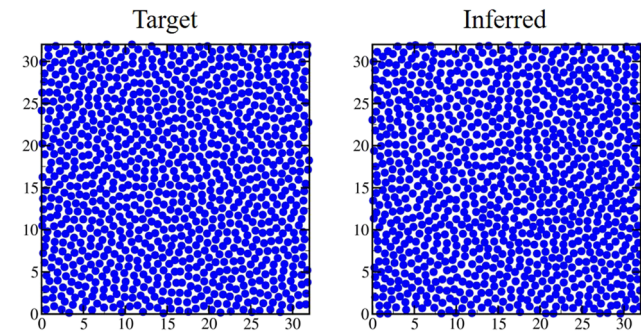


FIG. 11. Snapshots of the systems in Fig. 7. The target system has more “striped” features than the inferred system.

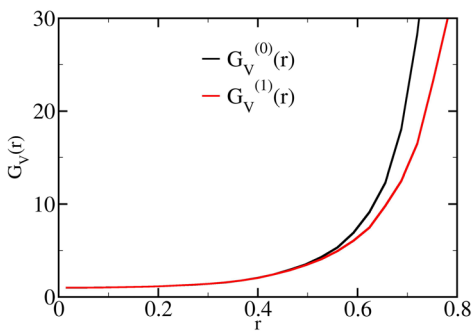


FIG. 12. Plot of the conditional nearest-neighbor distribution function $G_V(r)$ for the systems described in Fig. 7.

local density fluctuations, and it has more nearly linear chains of particles.

To quantify higher-order structural differences, we have computed the conditional nearest-neighbour distribution function $G_V(r)$ for both systems, defined as follows: Given that a spherical region $\Omega_V(r)$ of radius r is empty of particles, $\rho s_1(r)G_V(r)dr$ is the probability of finding particles in the spherical shell of volume $s_1(r)dr$ encompassing the cavity, where $s_1(r)$ is the surface area of a d -dimensional sphere of radius r .⁵⁹ It has been shown that $G_V(r)$ for general many-body systems can be explicitly expressed in terms of certain integrals involving the infinite set of many-body correlation functions $\{g_2, g_3, \dots\}$.⁶⁰ Figure 12 plots $G_V(r)$'s for the target and inferred systems described in Fig. 7. The two $G_V(r)$'s become increasingly different as r increases above 0.5. This implies that the higher-body correlation functions of the target and inferred systems are substantially different.

VII. EXTENSION OF HENDERSON'S THEOREM

In this section, we present a more general version of Henderson's theorem, extending the uniqueness statement to potentials that involve two- and higher-body interactions. Suppose the potential energy Φ of a many-body system involves at most n -body interactions,

$$\Phi(\mathbf{r}^N) = \sum_i^N \phi_1(\mathbf{r}_i) + \sum_{i < j}^N \phi_2(\mathbf{r}_i, \mathbf{r}_j) + \dots + \sum_{i < j < \dots < m}^N \phi_n(\mathbf{r}_i, \mathbf{r}_j, \dots, \mathbf{r}_m), \quad (22)$$

where ϕ_k is the k -body interaction term. The generalized Henderson theorem can be stated as follows:

Theorem 1 (Henderson). At fixed ρ , T , the potential Φ that produces a given set of equilibrium n -point probability density functions $\{\rho_1(\mathbf{r}), \dots, \rho_n(\mathbf{r}_1, \dots, \mathbf{r}_n)\}$ is unique up to an additive constant.

Proof. The proof is exactly analogous to Henderson's proof about pair correlation functions. For an ensemble α of point

configurations, the ensemble-averaged energy per particle can be expressed as

$$\frac{\langle \Phi \rangle_\alpha}{N} = \int \phi_1(\mathbf{r}) \langle \rho_1(\mathbf{r}) \rangle_\alpha d\mathbf{r} + \dots + \frac{1}{n!} \int \dots \times \int \phi_n(\mathbf{r}_1, \dots, \mathbf{r}_n) \langle \rho_n(\mathbf{r}_1, \dots, \mathbf{r}_n) \rangle_\alpha d\mathbf{r}_1 \dots d\mathbf{r}_n, \quad (23)$$

where $\langle \cdot \rangle_\alpha$ is the ensemble average. Let Φ_0, Φ_1 be two potentials involving up to n -body interactions that have the same equilibrium probability density functions, i.e., $\langle \rho_k \rangle_0 = \langle \rho_k \rangle_1$ for all k , where $\langle \cdot \rangle_0, \langle \cdot \rangle_1$ are the canonical ensemble averages corresponding to Φ_0 and Φ_1 , respectively. The Gibbs inequality states that for two probability distributions $w_0(\mathbf{r}^N)$ and $w_1(\mathbf{r}^N)$,

$$\int w_0 \ln w_1 d\mathbf{r}^N \leq \int w_0 \ln w_0 d\mathbf{r}^N, \quad (24)$$

where the equality holds if and only if $w_0 = w_1$. Let w_0, w_1 be the canonical probability distribution corresponding to Φ_0, Φ_1 , respectively, i.e., $w_\alpha = \exp(-\beta \Phi_\alpha)/\exp(-\beta \Phi_\alpha) d\mathbf{r}^N$, where $\beta = 1/k_B T$. At finite T , Eq. (24) gives

$$\frac{\langle \Phi_1 \rangle_1}{T} - S_1 = \frac{F_1}{T} \leq \frac{\langle \Phi_1 \rangle_0}{T} - S_0, \quad (25)$$

$$\frac{\langle \Phi_0 \rangle_0}{T} - S_0 = \frac{F_0}{T} \leq \frac{\langle \Phi_0 \rangle_1}{T} - S_1, \quad (26)$$

where $F_\alpha = -k_B T \ln \int \exp(-\beta \Phi_\alpha) d\mathbf{r}^N$ is the Helmholtz free energy and $S_\alpha = -f w_\alpha \ln w_\alpha d\mathbf{r}^N$ is the entropy. Adding Eqs. (25) and (26), and using the definition (9), we have

$$D_{JS} = \frac{\langle \Phi_0 - \Phi_1 \rangle_1}{T} - \frac{\langle \Phi_0 - \Phi_1 \rangle_0}{T} \geq 0, \quad (27)$$

and the equality holds if and only if $w_0 = w_1$. By assumption, $\langle \rho_k \rangle_0 = \langle \rho_k \rangle_1$ for all k , so $\langle \Phi_0 - \Phi_1 \rangle_0 = \langle \Phi_0 - \Phi_1 \rangle_1$ [Eq. (23)]. The equality in Eq. (27) holds, and we have $w_0 = w_1$. Due to the strict monotonicity of w_α with respect to Φ_α at positive T , we conclude that the potentials Φ_0 and Φ_1 differ by no more than an additive constant, which proves the theorem. \square

The practicality of the generalized Henderson theorem, i.e., the sensitivity of many-body correlation functions to many-body interactions, must be scrutinized as in this work. For states where it is practically applicable, the generalized theorem could potentially guide the inverse design of many-body systems with three-body interactions. This is especially important for particles constrained on a 2D surface, e.g., air–liquid interface,⁶¹ where many-body configurations can be relatively easily sampled, and g_3 or even g_4 is readily obtainable.⁶²

Although the proof of Henderson's theorem does not directly contain information about the sensitivity of pair statistics on pair potentials, one can show that the effect of the Gibbs inequality [Eq. (24)] on this sensitivity is insignificant, i.e., a small Jensen–Shannon divergence always corresponds to similar probability distributions. This is due to Pinsker's inequality, which states that the

total variation of two probability distributions w_0, w_1 is bounded above by $\sqrt{2D_{1,0}}$, where $D_{1,0}$ is the relative entropy of w_1 with respect to w_0 .^{63,64}

Therefore, for cases where pair statistics are insensitive to pair potentials, we postulate that the main cause is the low sensitivity of $w = \exp(-\beta\Phi)/\int \exp(-\beta\Phi) d\mathbf{r}^N$ with respect to Φ . Roughly speaking, the expression $Q := |\delta \exp(-\beta\Phi)/\delta\Phi| = \beta \exp(-\beta\Phi)$ correlates with the sensitivity of w on Φ , which apparently vanishes when $T = 0$ and $T = \infty$ for finite Φ .

We note that several prior papers have generalized Henderson's theorem along similar lines.^{65–68} However, our proof is simpler and shows that Henderson's original argument is directly generalizable to the many-body cases.

VIII. CONCLUDING REMARKS

The results that we have obtained provide helpful insights into inverse statistical mechanics problems where one attempts to find effective pair potentials that are consistent with given pair statistics. We have shown that Henderson's theorem does not imply uniqueness of solutions to inverse problems encountered in practice. Depending on the states and the pair statistics of interest, the inverse algorithm should be carefully chosen, and the solutions should be interpreted with caution. For fluids in general, $g_2(r)$ is insensitive to pair potentials at high temperatures for medium to high densities, and $S(k)$ is insensitive to pair potentials at high temperatures for both low and high densities. Therefore, for such portions of the phase diagrams, inverse algorithms are unlikely to capture the complete functional forms of the target interactions, which, by Henderson's theorem, are unique, in principle. Furthermore, since we have shown that $S(k)$'s are insensitive to $v(r)$ where it has small values [$S(k) < 0.01$ as a rule of thumb], it is crucial that target structure factors are extremely precise in these regions. If this is not possible, the solutions to inverse problems are effectively ambiguous. For crystals of the same ground state, we found that the sensitivities are generally low for $T < 0.5T_{melting}$, but we also found high-sensitivity cases, as shown in Fig. 9. Finally, we observed that states near phase transitions usually give high sensitivities. Our findings highlight the importance of incorporating information other than pair statistics to determine effective pair interactions, such as pressure.^{46–50}

It is theoretically desirable to analyze the differential $J(r, r') = dg_2(r)/dv(r')$. The quantity J corresponds to the curvature of the relative entropy.⁶⁹ However, our preliminary calculations of J for the cases in Sec. IV suggest that random noise in $g_2(r)$ usually results in the overestimation of the magnitude of J for $r' > 4$, where $|dv(r')|$ is small. It would be desirable to pursue such analysis in future studies with highly precise structural data.

Our work also has implications in the study of the dynamics of classical many-body systems (e.g., glass formation). Systems with the pair interactions shown in the middle panel of Fig. 7 have very similar $g_2(r)$'s but distinctly different higher-order correlation functions (see Sec. VI). Such differences should be reflected in individually distinct dynamics, which is a subject worthy of future study. Thus, the determination of effective pair interactions only from the pair statistics^{19–21,27,31} could produce misleading conclusions about non-equilibrium properties of a many-body system.

A further implication of our results concerns the choice of benchmark systems used to test inverse algorithms. The most common choices are dense LJ fluids and liquid aluminum under some model potential with multiple minima.^{19,27} As we have shown, these are systems for which C_{g_2} and C_S are small. For such states, the trial potential functions usually converge, as expected, because their functional forms can be varied significantly by changing the steepness of repulsive forces and positions of minima/maxima, without causing significant changes to the pair statistics. During the optimization of the trial potential, the algorithm is unlikely to encounter trial systems that are dramatically different from the target system, which may cause the trial potentials to diverge. On the other hand, states where C_{g_2} and C_S are large, such as those near phase transitions, would pose much more challenging with respect to convergence. During optimization, slight changes in trial potentials could lead to markedly different pair statistics. Trial potentials may diverge accordingly and be unable to arrive at a solution to the inverse problem. We observed this divergent behavior in IBI for liquid states close to the freezing point. Such states are rarely chosen as benchmarks for inverse algorithms, and we believe that research in this direction is worth pursuing.

Finally, we point out that Frommer *et al.* showed that Henderson's original proof incorrectly assumes that Gibbs's variational principle for finite volume extends to the thermodynamic limit.⁷⁰ The authors demonstrate that the uniqueness theorem is applicable to a strict subset of all superstable potentials,⁷¹ beyond which they could not prove or disprove Henderson's uniqueness theorem. Therefore, in the thermodynamic limit, there might exist some exotic superstable potentials, not in the aforementioned class, that exactly reproduce the pair statistics of the LJ potential. Such examples, if found, would provide strict violations of Henderson's theorem.

ACKNOWLEDGMENTS

This work was supported by the National Science Foundation under Award No. CBET-1701843.

DATA AVAILABILITY

The data that support the findings of this study are available from the corresponding author upon reasonable request.

REFERENCES

1. K. Van Workum and J. F. Douglas, "Symmetry, equivalence, and molecular self-assembly," *Phys. Rev. E* **73**, 031502 (2006).
2. S. Torquato, "Inverse optimization techniques for targeted self-assembly," *Soft Matter* **5**, 1157–1173 (2009).
3. H. Cohn and A. Kumar, "Algorithmic design of self-assembling structures," *Proc. Natl. Acad. Sci. U. S. A.* **106**, 9570–9575 (2009); [arXiv:0906.3550](https://arxiv.org/abs/0906.3550).
4. P. G. Bolhuis, A. A. Louis, J. P. Hansen, and E. J. Meijer, "Accurate effective pair potentials for polymer solutions," *J. Chem. Phys.* **114**, 4296–4311 (2001).
5. M. Müller, B. Solenthaler, R. Keiser, and M. Gross, "Particle-based fluid-fluid interaction," in Proceedings of the 2005 ACM SIGGRAPH/Eurographics Symposium on Computer Animation, 2005.
6. J. W. Mullinax and W. G. Noid, "A generalized-Yvon-Born-Green theory for determining coarse-grained interaction potentials," *J. Phys. Chem. C* **114**, 5661–5674 (2010).

- ⁷A. Savel'yev and G. A. Papoian, "Chemically accurate coarse graining of double-stranded DNA," *Proc. Natl. Acad. Sci. U. S. A.* **107**, 20340–20345 (2010).
- ⁸M. Mechelke and M. Habeck, "Estimation of interaction potentials through the configurational temperature formalism," *J. Chem. Theory Comput.* **9**, 5685–5692 (2013).
- ⁹R. L. Henderson, "A uniqueness theorem for fluid pair correlation functions," *Phys. Lett. A* **49**, 197–198 (1974).
- ¹⁰L. Koralov, "Existence of pair potential corresponding to specified density and pair correlation," *Lett. Math. Phys.* **71**, 135–148 (2005), here Koralov proves a similar theorem for the grand canonical ensemble, i.e. that there exist a unique pair potential and a unique value activity for a given pair of density and $g_2(r)$.
- ¹¹H. I. Ingólfsson, C. A. Lopez, J. J. Uusitalo, D. H. de Jong, S. M. Gopal, X. Periole, and S. J. Marrink, *Wiley Interdiscip. Rev.: Comput. Mol. Sci.* **4**, 225–248 (2014).
- ¹²A. Moradzadeh and N. R. Aluru, "Transfer-learning-based coarse-graining method for simple fluids: Toward deep inverse liquid-state theory," *J. Phys. Chem. Lett.* **10**, 1242–1250 (2019).
- ¹³A. E. Stones, R. P. Dullens, and D. G. Aarts, "Model-free measurement of the pair potential in colloidal fluids using optical microscopy," *Phys. Rev. Lett.* **123**, 098002 (2019); [arXiv:1901.04960](https://arxiv.org/abs/1901.04960).
- ¹⁴F. Theil, "A proof of crystallization in two dimensions," *Commun. Math. Phys.* **262**, 209–236 (2006).
- ¹⁵H. Cohn and A. Kumar, "Optimality and uniqueness of the Leech lattice among lattices," *Ann. Math.* **170**, 1003–1050 (2009); [arXiv:0403263 \[math\]](https://arxiv.org/abs/0403263).
- ¹⁶L. Nowack and S. A. Rice, "Sequential phase transitions and transient structured fluctuations in two-dimensional systems with a high-density Kagome lattice phase," *J. Chem. Phys.* **151**, 244504 (2019).
- ¹⁷R. L. McGreevy, "Reverse Monte Carlo modelling," *J. Phys.: Condens. Matter* **13**, R877 (2001).
- ¹⁸R. Potestio, "Is Henderson's theorem practically useful?," *J. Unsolved Quest.* **3**, 13 (2013).
- ¹⁹D. Levesque, J. J. Weis, and L. Reatto, "Pair interaction from structural data for dense classical liquids," *Phys. Rev. Lett.* **54**, 451–454 (1985).
- ²⁰A. P. Lyubartsev and A. Laaksonen, "Calculation of effective interaction potentials from radial distribution functions: A reverse Monte Carlo approach," *Phys. Rev. E* **52**, 3730–3737 (1995).
- ²¹A. K. Soper, "Empirical potential Monte Carlo simulation of fluid structure," *Chem. Phys.* **202**, 295–306 (1996).
- ²²C. N. Likos, "Effective interactions in soft condensed matter physics," *Phys. Rep.* **348**, 267–439 (2001).
- ²³A. K. Soper, "Tests of the empirical potential structure refinement method and a new method of application to neutron diffraction data on water," *Mol. Phys.* **99**, 1503–1516 (2001).
- ²⁴A. A. Louis, "Beware of density dependent pair potentials," *J. Phys.: Condens. Matter* **14**, 9187–9206 (2002).
- ²⁵F. H. Stillinger, H. Sakai, and S. Torquato, "Statistical mechanical models with effective potentials: Definitions, applications, and thermodynamic consequences," *J. Chem. Phys.* **117**, 288–296 (2002).
- ²⁶N. Almarza, E. Lomba, G. Ruiz, and C. Tejero, "Local density approach for modeling fluids with density-dependent interactions," *Phys. Rev. E* **67**, 021202 (2003).
- ²⁷M. D'Alessandro and F. Cilloco, "Information-theory-based solution of the inverse problem in classical statistical mechanics," *Phys. Rev. E* **82**, 021128 (2010).
- ²⁸A. A. Louis, "Extracting short-ranged interactions from structure factors," *Mol. Phys.* **109**, 2945–2951 (2011).
- ²⁹G. D'Adamo, A. Pelissetto, and C. Pierleoni, "Coarse-graining strategies in polymer solutions," *Soft Matter* **8**, 5151–5167 (2012).
- ³⁰J. McCarty, A. J. Clark, I. Y. Lyubimov, and M. G. Guenza, "Thermodynamic consistency between analytic integral equation theory and coarse-grained molecular dynamics simulations of homopolymer melts," *Macromolecules* **45**, 8482–8493 (2012).
- ³¹M. Habeck, "Bayesian approach to inverse statistical mechanics," *Phys. Rev. E* **89**, 052113 (2014).
- ³²M. Heinen, "Calculating particle pair potentials from fluid-state pair correlations: Iterative Ornstein-Zernike inversion," *J. Comput. Chem.* **39**, 1531–1543 (2018); [arXiv:1711.03630](https://arxiv.org/abs/1711.03630).
- ³³D. Wu, L. Wang, and P. Zhang, "Solving statistical mechanics using variational autoregressive networks," *Phys. Rev. Lett.* **122**, 080602 (2019); [arXiv:1809.10606](https://arxiv.org/abs/1809.10606).
- ³⁴S. Torquato, "Hyperuniform states of matter," *Phys. Rep.* **745**, 1–95 (2018).
- ³⁵A pair potential v is called stable if there exists some $B \geq 0$ such that the N -particle configurational energy $\Phi(\mathbf{r}^N) = \sum_i^N v(\mathbf{r}_i, \mathbf{r}_j) \geq NB$ for all N .
- ³⁶M. S. Shell, "The relative entropy is fundamental to multiscale and inverse thermodynamic problems," *J. Chem. Phys.* **129**, 144108 (2008).
- ³⁷R. D. Batten, F. H. Stillinger, and S. Torquato, "Interactions leading to disordered ground states and unusual low-temperature behavior," *Phys. Rev. E* **80**, 031105 (2009).
- ³⁸C. Hanel, C. N. Likos, and R. Blaak, "Effective interactions between multilayered ionic microgels," *Materials* **7**, 7689–7705 (2014).
- ³⁹C. N. Likos, H. Löwen, M. Watzlawek, B. Abbas, O. Jucknischke, J. Allgaier, and D. Richter, "Star polymers viewed as ultrasoft colloidal particles," *Phys. Rev. Lett.* **80**, 4450–4453 (1998).
- ⁴⁰Another class of the inverse problem aims at constructing configurations consistent with the pair correlation function, which can be solved by reverse Monte Carlo proposed by McGreevy, see Ref. 17.
- ⁴¹R. B. Jadrich, J. A. Bollinger, B. A. Lindquist, and T. M. Truskett, "Equilibrium cluster fluids: Pair interactions via inverse design," *Soft Matter* **11**, 9342 (2015); [arXiv:1507.06936](https://arxiv.org/abs/1507.06936).
- ⁴²R. L. McGreevy and L. Pusztai, "Reverse Monte Carlo simulation: A new technique for the determination of disordered structures," *Mol. Simul.* **1**, 359–367 (1988).
- ⁴³G. Zhang and S. Torquato, "Realizable hyperuniform and nonhyperuniform particle configurations with targeted spectral functions via effective pair interactions," *Phys. Rev. E* **101**, 032124 (2020).
- ⁴⁴B. Widom, "Intermolecular forces and the nature of the liquid state," *Science* **157**, 375–382 (1967).
- ⁴⁵D. Chandler, J. D. Weeks, and H. C. Andersen, "van der Waals picture of liquids, solids, and phase transformations," *Science* **220**, 787–794 (1983).
- ⁴⁶F. Müller-Plathe, "Coarse-graining in polymer simulation: From the atomistic to the mesoscopic scale and back," *ChemPhysChem* **3**, 754–769 (2002).
- ⁴⁷S. Jain, S. Garde, and S. K. Kumar, "Do inverse Monte Carlo algorithms yield thermodynamically consistent interaction potentials?," *Ind. Eng. Chem. Res.* **45**, 5614–5618 (2006).
- ⁴⁸H. Wang, C. Junghans, and K. Kremer, "Comparative atomistic and coarse-grained study of water: What do we lose by coarse-graining?," *Eur. Phys. J. E* **28**, 221–229 (2009).
- ⁴⁹T. C. Moore, C. R. Iacobella, and C. McCabe, "Derivation of coarse-grained potentials via multistate iterative Boltzmann inversion," *J. Chem. Phys.* **140**, 224104 (2014).
- ⁵⁰A.-T. Kuo, S. Okazaki, and W. Shinoda, "Transferable coarse-grained model for perfluorosulfonic acid polymer membranes," *J. Chem. Phys.* **147**, 094904 (2017).
- ⁵¹F. H. Stillinger, "Phase transitions in the Gaussian core system," *J. Chem. Phys.* **65**, 3968 (1976).
- ⁵²S. Prestipino, F. Saija, and P. V. Giaquinta, "Hexatic phase in the two-dimensional Gaussian-core model," *Phys. Rev. Lett.* **106**, 235701 (2011); [arXiv:1107.0828](https://arxiv.org/abs/1107.0828).
- ⁵³S. Torquato and F. H. Stillinger, "New conjectural lower bounds on the optimal density of sphere packings," *Exp. Math.* **15**, 307 (2006).
- ⁵⁴Y. Jiao, F. H. Stillinger, and S. Torquato, "Geometrical ambiguity of pair statistics: Point configurations," *Phys. Rev. E* **81**, 011105 (2010).
- ⁵⁵F. H. Stillinger and S. Torquato, "Structural degeneracy in pair distance distributions," *J. Chem. Phys.* **150**, 204125 (2019).
- ⁵⁶R. Evans, "Comment on reverse Monte Carlo simulation," *Mol. Simul.* **4**, 409–411 (1990).
- ⁵⁷A. P. Lyubartsev and A. Laaksonen, "Osmotic and activity coefficients from effective potentials for hydrated ions," *Phys. Rev. E* **55**, 5689–5696 (1997).
- ⁵⁸J. W. Mullinax and W. G. Noid, "Generalized Yvon-Born-Green theory for molecular systems," *Phys. Rev. Lett.* **103**, 198104 (2009).

- ⁵⁹S. Torquato, *Random Heterogeneous Materials* (Springer, 2002).
- ⁶⁰S. Torquato, B. Lu, and J. Rubinstein, “Nearest-neighbor distribution functions in many-body systems,” *Phys. Rev. A* **41**, 2059–2075 (1990).
- ⁶¹J. Toro-Mendoza, G. Rodriguez-Lopez, and O. Paredes-Altuve, “Brownian diffusion of a particle at an air/liquid interface: The elastic (not viscous) response of the surface,” *Phys. Chem. Chem. Phys.* **19**, 9092–9095 (2017).
- ⁶²H. Malmir, M. Sahimi, and Y. Jiao, “Higher-order correlation functions in disordered media: Computational algorithms and application to two-phase heterogeneous materials,” *Phys. Rev. E* **98**, 063317 (2018).
- ⁶³I. Csiszár and J. Körner, *Information Theory: Coding Theorems for Discrete Memoryless Systems* (Cambridge University Press, 2011).
- ⁶⁴The total variation of w_0 and w_1 is defined as $\delta(w_0, w_1) = \int |w_1 - w_0| dr^N$.
- ⁶⁵J. T. Chayes and L. Chayes, “On the validity of the inverse conjecture in classical density functional theory,” *J. Stat. Phys.* **36**, 471–488 (1984).
- ⁶⁶J. T. Chayes, L. Chayes, and E. H. Lieb, “The inverse problem in classical statistical mechanics,” *Commun. Math. Phys.* **93**, 57–121 (1984).
- ⁶⁷M. E. Johnson, T. Head-Gordon, and A. A. Louis, “Representability problems for coarse-grained water potentials,” *J. Chem. Phys.* **126**, 144509 (2007).
- ⁶⁸J. F. Rudzinski and W. G. Noid, “Coarse-graining entropy, forces, and structures,” *J. Chem. Phys.* **135**, 214101 (2011).
- ⁶⁹T. Murtola, M. Karttunen, and I. Vattulainen, “Systematic coarse graining from structure using internal states: Application to phospholipid/cholesterol bilayer,” *J. Chem. Phys.* **131**, 055101 (2009).
- ⁷⁰F. Frommer, M. Hanke, and S. Jansen, “A note on the uniqueness result for the inverse Henderson problem,” *J. Math. Phys.* **60**, 093303 (2019); [arXiv:1903.03317](https://arxiv.org/abs/1903.03317).
- ⁷¹A superstable potential is a potential that can be written as a sum of a stable potential v' and a non-negative function v'' such that $v''(0) > 0$, see Ref. 72.
- ⁷²D. Ruelle, “Superstable interactions in classical statistical mechanics,” *Commun. Math. Phys.* **18**, 127 (1970).